International Journal of Industrial and Manufacturing Systems Engineering
2019; 4(6): 54-63
http://www.sciencepublishinggroup.com/j/ijimse
doi: 10.11648/j.ijimse.20190406.11
ISSN: 2575-3150 (Print); ISSN: 2575-3142 (Online)

Modeling of Integrated Octagonal Planar Transformer for RF Systems

Mokhtaria Derkaoui

LaRATIC Laboratory, National Institute of Telecommunicati, Ons & ICT, INTTIC, Oran, Algeria

Email address:
mderkaoui@inttic.dz

To cite this article:
Mokhtaria Derkaoui. Modeling of Integrated Octagonal Planar Transformer for RF Systems. *International Journal of Industrial and Manufacturing Systems Engineering*. Vol. 4, No. 6, 2019, pp. 54-63. doi: 10.11648/j.ijimse.20190406.11

Received: October 7, 2019; **Accepted**: November 14, 2019; **Published**: November 22, 2019

Abstract: One of the important components in many RF ICs applications is the transformer. It is very important that transformer has optimal design, that means, optimal geometry with the best possible characteristics. Because of the wide transformer applications in radio-frequency silicon-based circuits, modeling for transformers has become more and more essential. The modeling of planar transformer for very high frequencies is the subject of this paper. Square, polygonal and circular shapes of the planar windings are the important difference regarding transformer topologies. In this work, comparison was restricted to a square and an octagonal shape of the windings. In this study, we opted for calculation method developed by Wheeler to evaluate the inductance of different planar geometrical shapes of transformer windings. Besides, we determined the geometrical parameters of the transformer and from its π-electrical model; we highlighted all parasitic effects generated by stacking of different material layers. By using the S-parameters, we calculated the technological parameters. The important characteristics of a transformer are its inductances values and its parasitic capacitances and resistances, which determine its Q factor and self-resonant frequency. Furthermore, we carried out the electromagnetic simulation using COMSOL Multiphysics 4.3 software to show current density and electromagnetic field in the windings of the transformer for high frequencies.

Keywords: Integration, Transformer, Octagonal, On-chip, Planar, RF

1. Introduction

Perpetual miniaturization of electronic components makes it possible to load more and more portable consumer equipment and accessories in various fields, transport, telecommunication, computer science, …etc. The whole integration of energy conversion devices designed to create compact power circuits is now experiencing strong technological constraints. It is the same for the inductive and capacitive components integration due to their encumber in surface and volume. The decreased size and increased operational frequency caused off-chip passive devices to be the major obstacle in the way to reducing the total system size. The common sense solution is to move the passive components, like capacitors, inductors, and transformers, from the board to the chip realm. The first implementation of monolithic inductors on silicon substrates for mixed-signal radio-frequency ICs circuits was achieved [1, 2], making the use of integrated passive components practical. A few years later, advantages of using monolithic transformers in the design of low-voltage silicon bipolar receivers were demonstrated by [3, 4].

In the last years, monolithic transformers have been successfully implemented in RFIC designs [5, 6] enabling the implementation of high frequency circuits such as mixers, voltage-controlled oscillators, low noise amplifiers. Because of the wide application of transformers in RF systems circuits, modelling for transformers has become more and more essential.

2. Windings Modeling of an Inductive Device

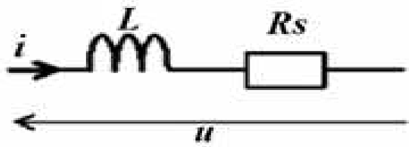

Figure 1. *Simplified model of a low frequency inductor.*

An inductor is modeled by a pure inductance in series with a resistance Rs, which characterizes the different losses in the component in low frequencies (Figure 1).

In high frequencies (from 100 MHz), inter-winding capacitive couplings can no longer be neglected. The behavior of the inductor can be represented by an ideal inductance L in series with a resistance Rs and in parallel with an ideal capacitance Cs for the global taking into account of the capacitive coupling between turns (Figure 2).

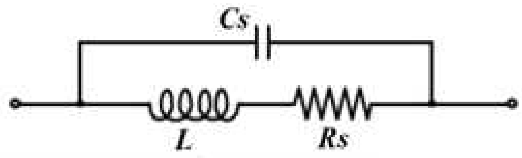

Figure 2. *Model of a high frequency inductor.*

Nguyen and Meyer [7] were the first to propose a simple model in "π" to describe the behavior of an integrated planar inductor on silicon (Figure 3), Ashby and al [8] developed an improved model. Whereas, the parameters of the model need to be adjusted from the experimental data. Then, Yue and Yong [9] present a similar model (Figure 4a), but with more appropriate parameters for the geometry of the inductance. The electrical diagram of a planar spiral inductor is derived from its cross-section (Figure 4b). In this case, the capacitance Cs makes it possible to take into account the capacitive couplings between the turns. Capacitance Cox represent the coupling between the conductor and the substrate.

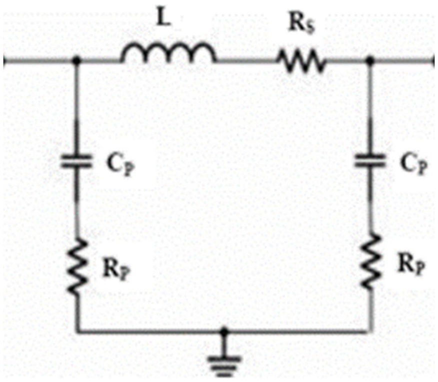

Figure 3. *Model in π developed by Nguyen et Meyer [7].*

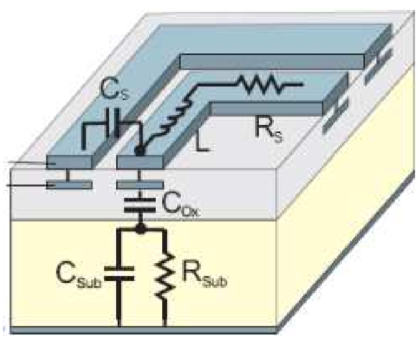

(a)

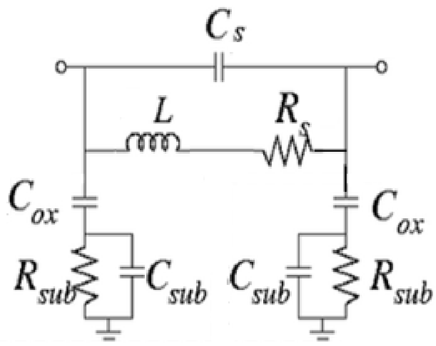

(b)

Figure 4. *Planar inductor developed by Yue and Yong [9]: (a) Cross-section, (b) Model in π.*

When a magnetic material layer is placed above or below the inductance, the model becomes very complicated because of the interactions between the stacking layers constituting the inductor (winding-magnetic material-substrate). The first equivalent scheme (Figure 5) was proposed by Yamaguchi and al. [10, 11].

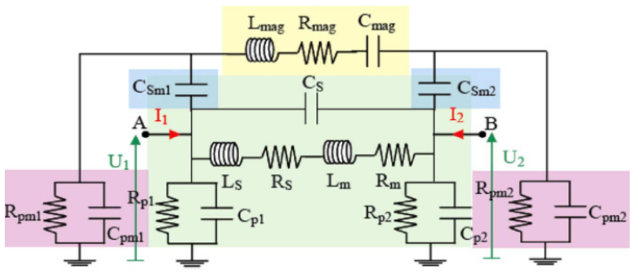

Figure 5. *π electrical model of a ferromagnetic inductor [10, 11].*

The work proposed by [12-14] in Figure 6 simplifies the electric diagram presented by [10], which shows the π model of a planar spiral inductor on a magnetic material. The different layers of the different materials superimposed and used in the manufacture of the integrated inductor are represented by the resistances and capacitances.

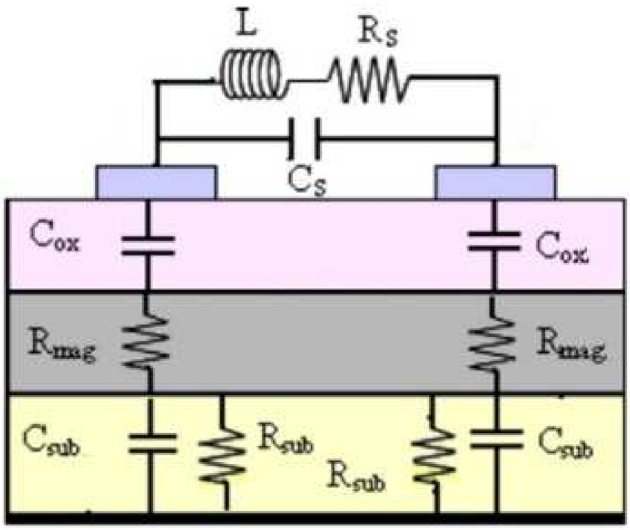

(a)

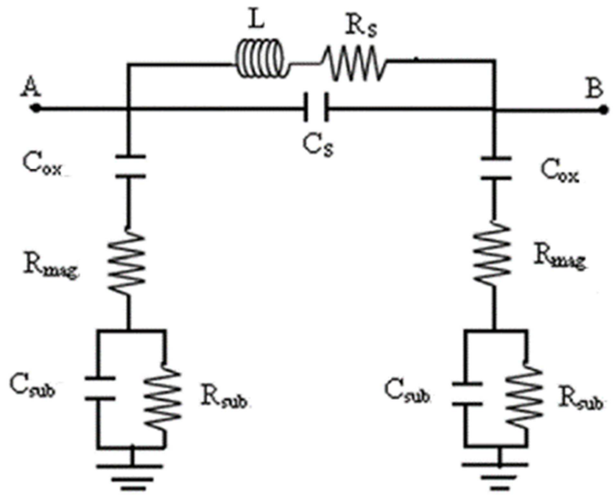

(b)

Figure 6. *Planar inductor on ferrite developed by [12-14]: (a) Cross-section, (b) Model in π.*

A transformer can be considered a device, whose operation is based on mutual inductive coupling between two coils. Figure 7 shows a schematic diagram of an ideal transformer.

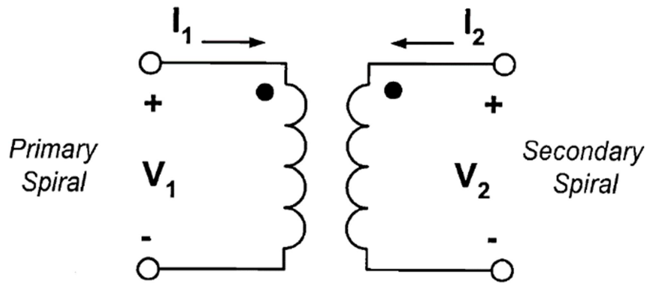

Figure 7. *Schematic diagram of a transformer.*

The work proposed by [15] shows the integrated transformer, which is composed of two planar windings of spiral square form. The two copper windings are deposited on a layer of ferrite magnetic material (NiZn), isolated therefrom by an insulating layer of silicon dioxide (SiO_2). The three layers are deposited on a silicon layer (Si) which serves as a substrate. A silicon dioxide layer of (SiO_2) which ensures the magnetic coupling separates the two stacks. The combination of the equivalent electrical circuits of two windings form the equivalent electrical circuit of transformer (Figure 8).

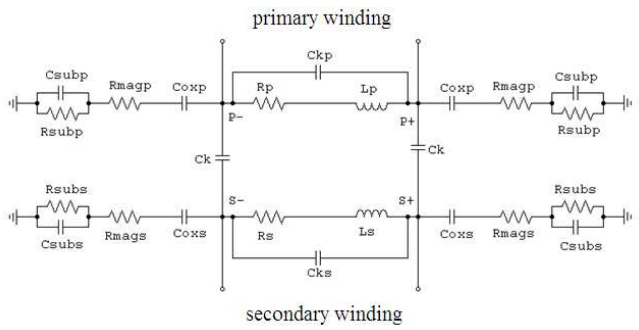

Figure 8. *Equivalent electrical circuit of integrated planar transformer [15].*

In this work, we present the model of a transformer whose windings are of octagonal planar shape (Figure 9a). The transformer is composed of two octagonal winding superimposed on a ferrite layer and isolated by a dioxide layer of silicon dioxide, all the layers of the different materials are superimposed on a layer of silicon, which serves as a substrate, this transformer operates at a high frequency of the order of 100 MHz. The (Figure 9b) presents the equivalent electrical circuit of the octagonal transformer.

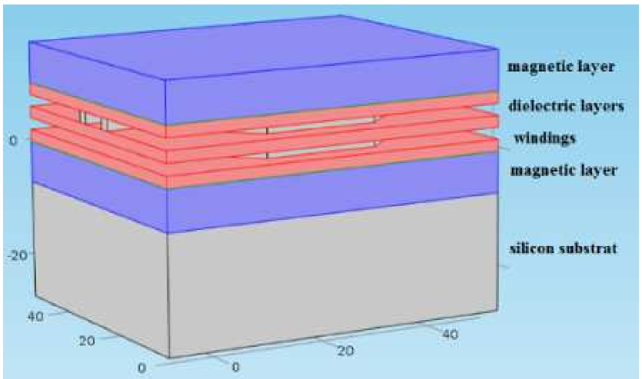

(a)

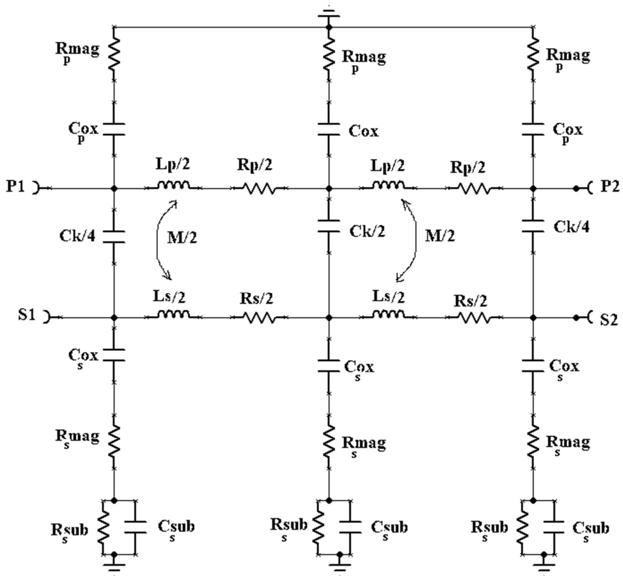

(b)

Figure 9. *Integrated planar octagonal transformer: (a) cross section, (b) equivalent electrical circuit.*

3. Electrical Parameters Calculation

The equivalent circuit of Figure 4 contains for the two windings the inductances L_p and L_s, serial resistances R_p and R_s, oxide capacitances C_{oxp}, C_{oxs}, magnetic layer resistances R_{magp}, R_{mags}, silicon substrate resistances R_{subp}, R_{subs}, silicon substrate capacitance C_{subp}, C_{subs}, coupling capacitance C_k between the two windings.

The analytical expressions of different elements are:

3.1. Serial Resistance of the Two Windings

$$R_p = \rho_{cu}.\frac{lt_p}{w_p.t} = 0.74\ \Omega \quad (1)$$

$$R_s = \rho_{cu}.\frac{lt_s}{w_s.t} = 0.045\ \Omega \quad (2)$$

$$\rho_{Cu} = 1.7.10^{-8}\ \Omega.m$$

3.2. Resistance of the Magnetic Layer

$$R_{magp} = 2.\rho_{NiZn}.\frac{e_{NiZn}}{w_p.l_{tp}} = 3.6\ k\Omega \quad (3)$$

$$R_{mags} = 2.\rho_{NiZn}.\frac{e_{NiZn}}{w_s.l_{ts}} = 2.06\ k\Omega \quad (4)$$

$$\rho_{NiZn} = 10^3\Omega.m$$

3.3. Resistances Associated to the Silicon Substrate

$$R_{subp} = 2.\rho_{Si}.\frac{e_{Si}}{w_p.l_{tp}} = 2.15\ k\Omega \quad (5)$$

$$R_{subs} = 2.\rho_{Si}.\frac{e_{Si}}{w_s.l_{ts}} = 1.22\ k\Omega \quad (6)$$

$$\rho_{Si} = 18.5\ \Omega.m$$

3.4. Oxide Capacitance

$$C_{oxp} = \frac{1}{2}.\varepsilon_0\varepsilon_{rox}.\frac{w_p.l_{tp}}{t_{ox}} = 2.97\ pF \quad (7)$$

$$C_{oxp} = \frac{1}{2}.\varepsilon_0\varepsilon_{rox}.\frac{w_s.l_{ts}}{t_{ox}} = 5.2\ pF \quad (8)$$

$$\varepsilon_{rox} = 3.9$$

3.5. Capacitance Associated to the Silicon Substrate

$$C_{subp} = \frac{1}{2}.\varepsilon_0\varepsilon_{rSi}.\frac{w_p.l_{tp}}{e_{si}} = 0.89\ pF \quad (9)$$

$$C_{subs} = \frac{1}{2}.\varepsilon_0\varepsilon_{rSi}.\frac{w_s.l_{ts}}{e_{si}} = 1.57\ pF \quad (10)$$

$$\varepsilon_{rSi} = 11.8$$

3.6. Coupling Capacitance Between the Two Windings

$$C_k = \varepsilon_0\varepsilon_{r\,air}.\frac{d_{out}^2}{t_{ox}} = 0.34\ fF \quad (11)$$

$$\varepsilon_{r\,air} = 1$$

In this work, we let the same values of the different geometric parameters (primary and secondary thickness t_p, t_s; width w_p, w_s; spacing s_p, s_s and total length lt_p, lt_s) calculated by [15]; we change the square form into an octagonal form.

In the expressions 1 to 11, we notice that all the values of the capacities are very weak; oxide capacities serve to avoid current infiltration into the magnetic core and into the substrate; inter-turns and coupling capacities avoid short-circuits between windings. Concerning the resistances, we see that the values of the resistances of magnetic core and the substrate are very high because they serve to limit the induced current by capacitive effect. However, the values of the series resistances of the windings are very weak to minimize the losses by Joule effects and facilitate the circulation of the current in the windings.

4. Calculation of the Inductances Values

The windings of the transformer are planar and the inductance value of each one depend of the inner and outer diameters d_{in} and d_{out} and their average d_{avg} (expression 12)

$$davg = (dout + din)/2 \quad (12)$$

The method of calculation developed by Wheeler allows an evaluation of the inductance of hexagonal, octagonal or square coil, realized in a discrete way [16]. A simplification can be made when one transposes in the integrated planar case [17]. The inductance L_{mw} given by Wheeler method is represented by (expression 13),

$$L_{mw} = k_1\mu_0\frac{n^2 d_{avg}}{1+k_2A_m} \quad (13)$$

A_m: the form factor (expression 14),

$$A_m = \frac{d_{out}-d_{in}}{d_{out}+d_{in}} \quad (14)$$

The coefficients k_1 and k_2 depend on the geometrical form used. The values of these coefficients are given in Table 1.

Table 1. *Values of coefficients k_1 and k_2 used in Wheeler method.*

Form	k1	k2
Square	2.34	2.75
Hexagonal	2.33	3.82
octagonal	2.25	3.55

According to the form factor A_m, it is possible to obtain so called “hollow” or “full” inductors (d_{out}>>d_{in}). Thus, a “full” inductor has a lower inductance than a “hollow” one because the turns located near the center of the spiral contribute to decrease the mutual positive inductances and increase the mutual negative inductances [18].

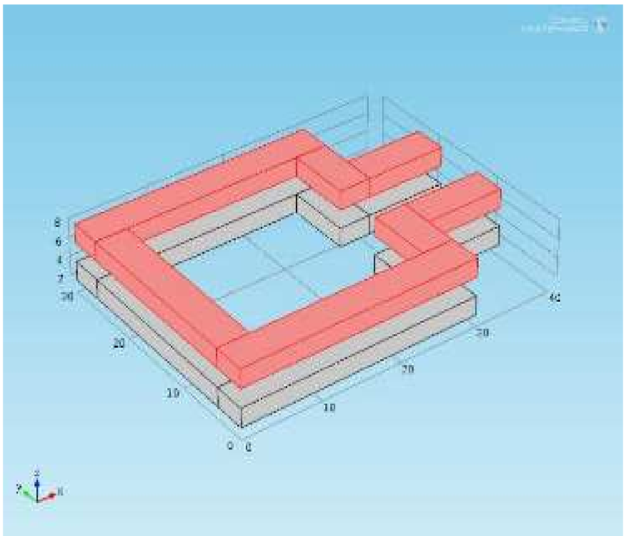

(a)

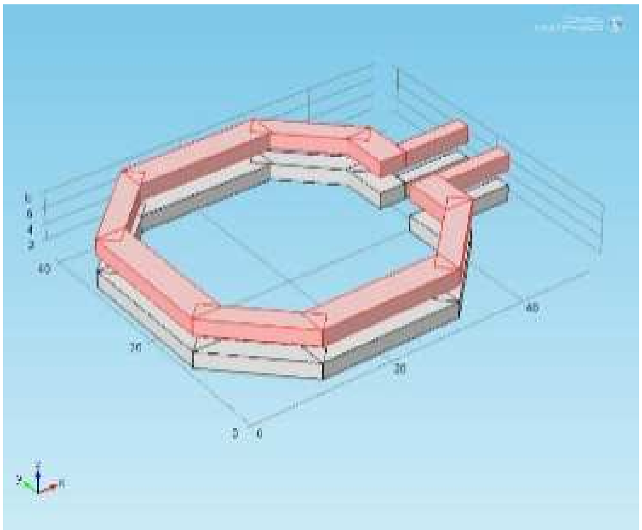

(b)

Figure 10. *(a) Square and (b) octagonal topologies.*

We have opted for an outer diameter of 2000 µm and a width of 50 µm. The shape of the windings is an important distinction regarding transformer topologies. Circular, square and polygonal spirals have already been reported to constitute inductors and transformers. In this study, comparison was hence restricted to a square (Figure 10a) and an octagonal transformer (Figure 10b) and angles are limited to multiples of 45 degrees.

5. S-parameters Concept

From the localized model we can easily obtain the scattering parameters of the transformer. The S-parameters of Figure 9b are calculated as follows [19]:

a) We calculate the ABCD matrices for each block.

$$\begin{bmatrix} A & B \\ C & D \end{bmatrix}_\alpha = \begin{bmatrix} 1 & 0 \\ \dfrac{1}{\frac{1}{j\omega C_{oxp}} + R_{magp} + \frac{R_{subp}}{1 + j\omega R_{subp} C_{subp}}} & 1 \end{bmatrix} \quad (15)$$

$$\begin{bmatrix} A & B \\ C & D \end{bmatrix}_\beta = \begin{bmatrix} 1 & R_{sp} \\ 0 & 1 \end{bmatrix} \quad (16)$$

$$\begin{bmatrix} A & B \\ C & D \end{bmatrix}_\gamma = -\begin{bmatrix} \frac{L_p}{M} & j\omega\left(\frac{L_p.L_s}{M} - M\right) \\ \frac{1}{j\omega M} & \frac{L_s}{M} \end{bmatrix} \quad (17)$$

$$\begin{bmatrix} A & B \\ C & D \end{bmatrix}_\delta = \begin{bmatrix} 1 & R_{ss} \\ 0 & 1 \end{bmatrix} \quad (18)$$

$$\begin{bmatrix} A & B \\ C & D \end{bmatrix}_\varepsilon = \begin{bmatrix} 1 & 0 \\ \dfrac{1}{\frac{1}{j\omega C_{oxs}} + R_{mags} + \frac{R_{subs}}{1 + j\omega R_{subs} C_{subs}}} & 1 \end{bmatrix} \quad (19)$$

$$\begin{bmatrix} A & B \\ C & D \end{bmatrix}_\varphi = \begin{bmatrix} 1 & \frac{1}{j\omega C_k} \\ 0 & 1 \end{bmatrix} \quad (20)$$

Where

$$M = k.\sqrt{L_p.L_s} \quad (21)$$

b) We can combine the blocks α, β, γ, δ, ε, φ in cascade:

$$\begin{bmatrix} A & B \\ C & D \end{bmatrix}_I = \begin{bmatrix} A & B \\ C & D \end{bmatrix}_\alpha . \begin{bmatrix} A & B \\ C & D \end{bmatrix}_\beta . \begin{bmatrix} A & B \\ C & D \end{bmatrix}_\gamma . \begin{bmatrix} A & B \\ C & D \end{bmatrix}_\delta . \begin{bmatrix} A & B \\ C & D \end{bmatrix}_\varepsilon . \begin{bmatrix} A & B \\ C & D \end{bmatrix}_\varphi \quad (22)$$

c) We can combine the large intermediate block I with block φ in parallel. The final ABCD matrix of the entire transformer F is given below:

$$\begin{bmatrix} A & B \\ C & D \end{bmatrix}_F = \frac{1}{B_I + B_\varphi} . \begin{bmatrix} A_I B_\varphi + A_\varphi B_I & B_I . B_\varphi \\ (C_I + C_\varphi).(B_\varphi + B_I) + (D_I - D_\varphi).(A_\varphi - A_I) & D_\varphi B_I + D_I B_\varphi \end{bmatrix} \quad (23)$$

d) We can convert the A, B, C, D parameters to S-parameters as follows:

$$S_{11} = \frac{A_F + \frac{B_F}{Z_0} - C_F.Z_0 - D_F}{A_F + \frac{B_F}{Z_0} + C_F.Z_0 + D_F} \quad S_{12} = \frac{2.(A_F.D_F - (B_F.C_F))}{A_F + \frac{B_F}{Z_0} + C_F.Z_0 + D_F} \quad (24)$$

$$S_{21} = \frac{2}{A_F + \frac{B_F}{Z_0} + C_F.Z_0 + D_F} \quad S_{22} = \frac{-A_F + \frac{B_F}{Z_0} - C_F.Z_0 + D_F}{A_F + \frac{B_F}{Z_0} + C_F.Z_0 + D_F} \quad (25)$$

Z_0 is the characteristic impedance of the line. We note that due to reciprocity, we will have $A_F.D_F\text{-}B_F.C_F = 1$; thus, $S_{12}=S_{21}$.

From the S-parameters, we can determine the Z-parameters such that:

$$Z_{11} = Z_0.\frac{(1+S_{11}).(1-S_{22})+S_{21}.S_{12}}{(1-S_{11}).(1-S_{22})-S_{21}.S_{12}} \quad (26)$$

$$Z_{12} = Z_0.\frac{2.S_{12}}{(1-S_{11}).(1-S_{22})-S_{21}.S_{12}} \quad (27)$$

$$Z_{21} = Z_0.\frac{2.S_{21}}{(1-S_{11}).(1-S_{22})-S_{21}.S_{12}} \quad (28)$$

$$Z_{22} = Z_0.\frac{(1-S_{11}).(1+S_{22})+S_{21}.S_{12}}{(1-S_{11}).(1-S_{22})-S_{21}.S_{12}} \quad (29)$$

From the Z-parameters, we can determine the primary and secondary inductances and resistances (expressions 30 and 31),

$$L_p = \frac{Im(Z_{11})}{\omega} \quad L_s = \frac{Im(Z_{22})}{\omega} \quad (30)$$

$$R_p = Re(Z_{11}) \quad R_s = Re(Z_{22}) \quad (31)$$

The measurement results for square [15] and octagonal transformers are shown in Figure 11. Those two transformers present the same diameter and the same trace width. It is observed that for the same diameter, square windings present a higher inductance value. This difference is due to the greater total length the square device presents.

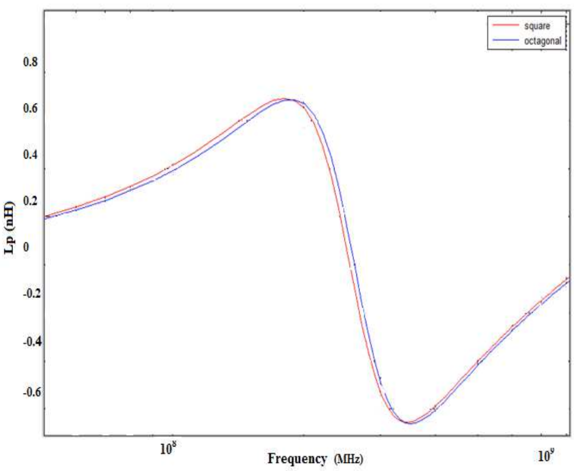

Figure 11. Measured inductances of square and octagonal transformers.

We also observe the characteristics of inductance behavior. We notice that there are three distinct zones: The inductive behavior up to 100 MHz operating frequency, a transition zone in which the value of the inductances becomes negative with a zero crossing corresponding to the own resonant frequency of the inductance and finally the capacitive behavior.

6. Quality Factor

The quality factor expresses losses of power in the windings of the transformer; it is defined as following [20]:

$$Q = 2\pi.\frac{\text{stocked energy}}{\text{dissipate denergy}} \quad (32)$$

For the inductor, only the stored energy in magnetic form is interesting. The quality factor is also proportional to the difference between the maximum magnetic energy and the energy supply, therefore the quality factor will be represented by the following relation [21, 22]:

$$Q = \frac{\omega.L}{R_s}.\frac{R_p}{R_p+\left[\left(\frac{\omega.L}{R_s}\right)^2+1\right]R_s}.\left[1-\frac{R_s^2(C_s+C_p)}{L}-\omega^2 L\left(C_s+C_p\right)\right] \quad (33)$$

In expression 33, we note that the first term corresponds to the simplified quality factor, the second term represents the losses substrate and the third expresses the self-resonance factor, ω is the pulsation, L is the inductance, Rs is the serial resistance, Cs is the serial capacitance, Rp is the coupling resistance and Cp the coupling capacitance. Rp and Cp are related to the resistance of the substrate R_{Si}, the capacitance of the substrate C_{si} and the oxide capacitance C_{ox} by the following expressions 34 and 35:

$$R_p = \frac{1}{\omega^2 C_{ox}^2 R_{si}} + \frac{R_{si}\left(C_{ox}+C_p\right)^2}{C_{ox}^2} \quad (34)$$

$$C_p = C_{ox}\frac{1+\omega^2\left(C_{ox}+C_{si}\right)C_{si}R_{si}^2}{1+\omega^2\left(C_{ox}+C_{si}\right)^2 R_{si}^2} \quad (35)$$

The following expressions determine the quality factors of primary and secondary windings;

$$Q_p = \frac{\mathrm{Im}(Z_{11})}{\mathrm{Re}(Z_{11})}\; Q_s = \frac{\mathrm{Im}(Z_{22})}{\mathrm{Re}(Z_{22})} \quad (36)$$

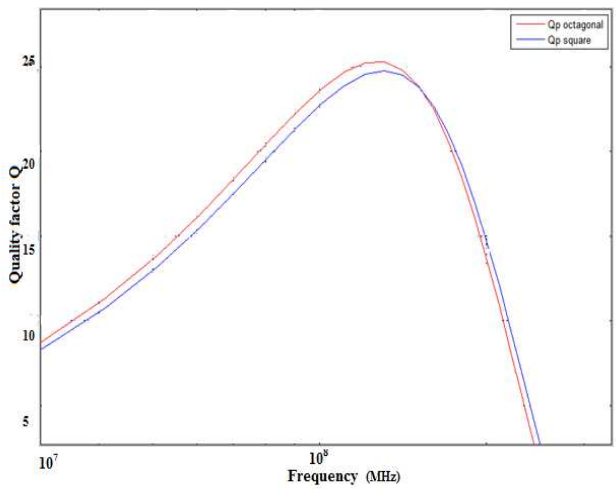

Figure 12. Quality factors of square and octagonal transformers.

The measurement results of quality factors of secondary square [15] and octagonal windings are shown in Figure 12. The two components present the same diameter and the same trace width. We note that octagonal transformers have lightly better quality factor. This means that the reduction of this topology brings to the resistance and capacitance of the windings is proportionally more substantial than the reduction on the inductance.

We also note that the quality factor increases with the frequency until reaching a maximum value which corresponds to the losses. The first part of the curve corresponds to the zone where the windings have an inductive behavior. Beyond this frequency, the quality factor decreases to zero at an operating point corresponding to the resonant frequency.

7. Feed Lines Position

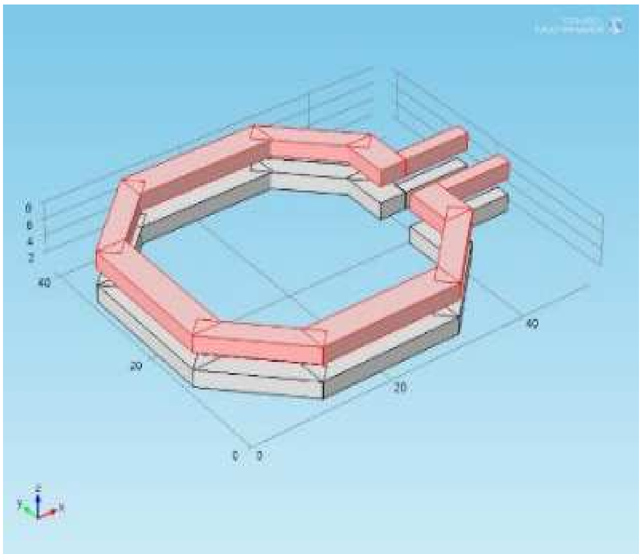

(a)

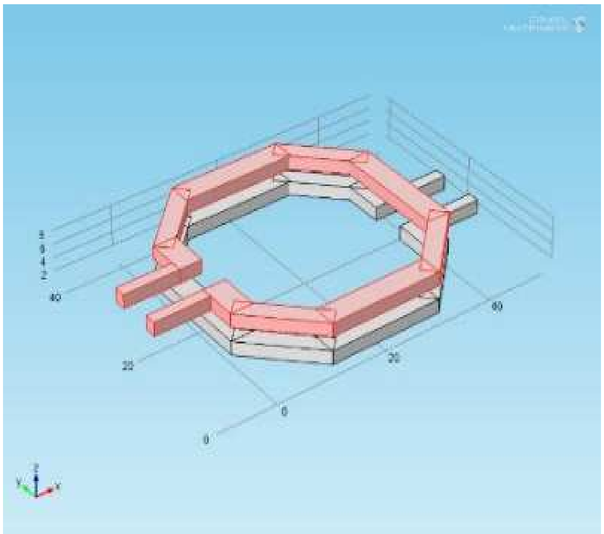

(b)

Figure 13. *(a) Non-flipped and (b) flipped transformer topologies.*

As the stacked topology is adopted, the relative position between primary and secondary is also considered in terms of the location of their respective leads. One approach is to have the secondary completely covered by the primary, so that their feed lines overlap (Figure 13a). Another flipped transformer possibility consists in a 180-degree rotation of one of the windings (Figure 13b). This conFigureuration results in an uncovered zone of the windings, which tends to weaken their coupling. The choice between these structures should be made not only in function of their performance but also considering which one is better suited to the layout of a specific circuit.

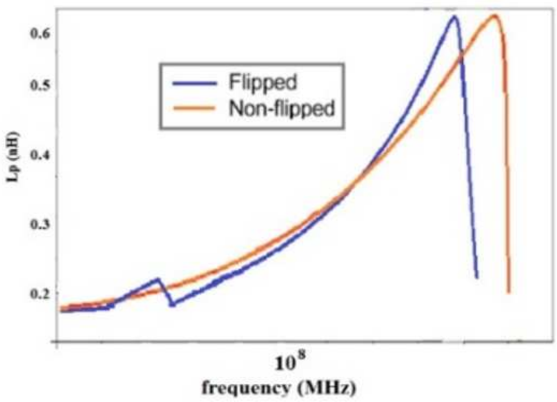

Figure 14. *Flipped and non-flipped inductances.*

The measurement results for transformers with those two topologies are presented in Figure 14. The obtained curves show a significant reduction of the resonant frequency of the transformer when the flipped topology is adopted. Since low frequency, self-inductances remain unchanged and magnetic coupling is weakened, this reduction results mostly from the augmented oxide and substrate capacitance that this topology presents. Even though magnetic coupling is significantly lower, global coupling including capacitive effects presents similar results beyond 100 MHz. It is also noticed that the flipped transformer demonstrates a lower minimum insertion loss for frequencies greater than 100 MHz, however the non-flipped transformer presents a proper performance for a wider band.

8. Geometric Dimensions

When the general topology of a transformer is defined, it is necessary to examine the sizing of the component and to show the influence of the different geometric dimensions of the windings on the transformer performances. Initially, the impact of the winding diameter is considered. Two transformers presenting the exact same topology but different average diameters were compared. They were laid out in a flipped conFigureuration with octagonal windings and 8-µm wide traces.

Figure 15 presents the measurement results with the considered diameters 50µm and 60µm. As the increased diameter is directly reflected in an increased total electric length, the obtained results reinforce the direct dependency between length and the low frequency inductance value. Concerning the quality factors, we observe that their maximum values remain unchanged before the partial resonance. Beyond this frequency, the Q factor is superior for the smaller transformer. For this reason, the measured minimum insertion loss is equivalent for the two transformers in the vicinity of 100 MHz. Therefore, we can conclude that for the same topology and conductor width, the choice of the transformers diameter for an integrated circuit should mostly rely on the desired inductance and occupied surface.

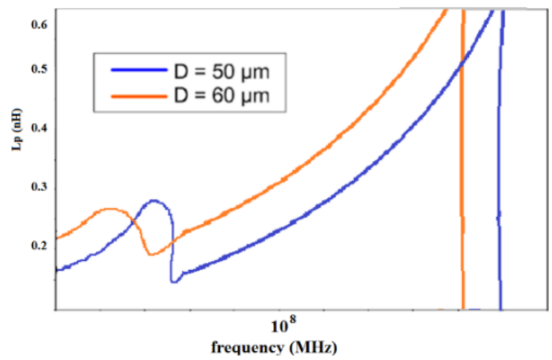

(a)

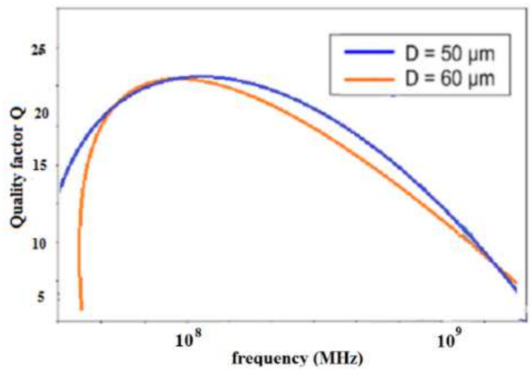

(b)

Figure 15. *(a) Inductances, (b) quality-factors with different diameters.*

Afterwards, the trace width of conductors was analyzed. This study was based on measurements of two transformers, with the same average diameter (60µm) and non-flipped topology. Their respective widths were 4µm and 12µm. Obtained measurement results are represented in Figure 16. We notice a linear effect of the width on the inductance; the inductance is higher when the traces are narrower. The influence on the quality factors, on the other hand, is not so straightforward. Results show that Q factors vary as frequency increases, so that for lower frequencies the 12µm wide transformer has a better Q, however the quality factor of the 4µm wide transformer is superior for higher frequencies. The resonant frequency of the transformer is not significantly affected, since the augmentation of the inductance for narrow traces is compensated by a reduction on the equivalent capacitance, which is related to the surface occupied by the transformer.

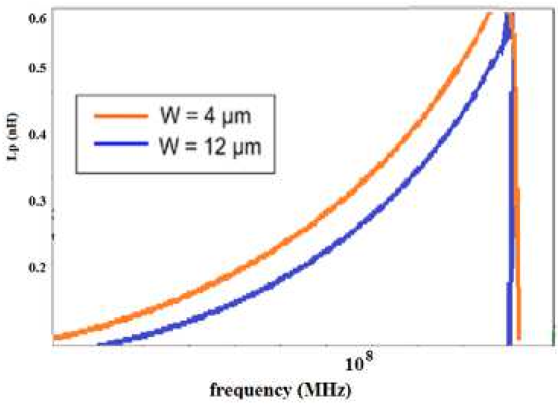

(a)

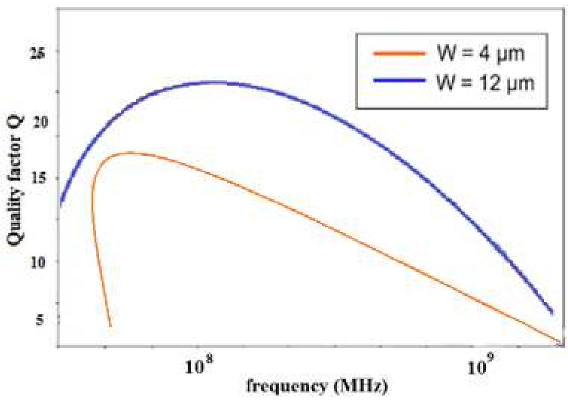

(b)

Figure 16. *(a) Inductances, (b) quality factors with different widths.*

9. 3D Simulation of the Electromagnetic Effects

In this section, we present 3D simulation of electromagnetic effects on the transformers at 100 MHz using software COMSOL Multiphysics 4.3 which is based on finite elements method.

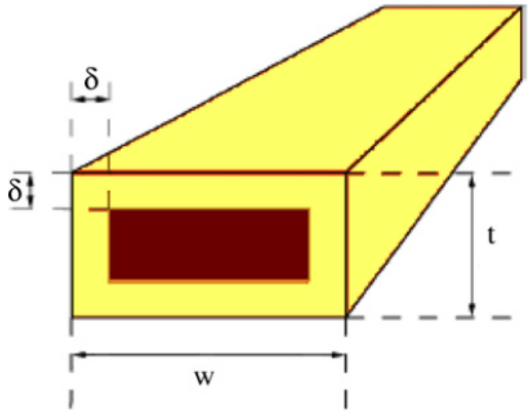

Figure 17. *Volume delimited by the skin effect δ in a conductor.*

In the conductor, the current density whose section is rectangular (Figure 17), is expressed by the following expressions [23],

$$j(x) = j_0 . e^{-i\left(\frac{x}{\delta}\right)} . e^{-\left(\frac{x}{\delta}\right)} \tag{37}$$

$$\|j(x)\| = j_0 . e^{-\left(\frac{x}{\delta}\right)} \tag{38}$$

The average value of the current density is given by:

$$j_{moy} = j_0 . \frac{\left[e^{-\left(\frac{t}{2\delta}\right)} + 1\right]}{2} \tag{39}$$

The current flowing in the winding of the transformer that we want to integrate is a function of the cross section of the conductor S_c and the current density j_{moy}. It is given by the following expression:

$$i_p = S_c . j_{moy} \tag{40}$$

The section S_c of the turn of the transformer is rectangular; it is given by the following expression:

$$S_c = w . t \tag{41}$$

Skin effect is patent for the considered conductors. Figure 18 shows the electromagnetic simulation of the current density on the two transformers at 100 MHz. It is clearly noticed how, even for the 4µm width of transformer, current is mostly concentrated on the edges of the conductors. This effect contributes to limiting the attainable insertion losses.

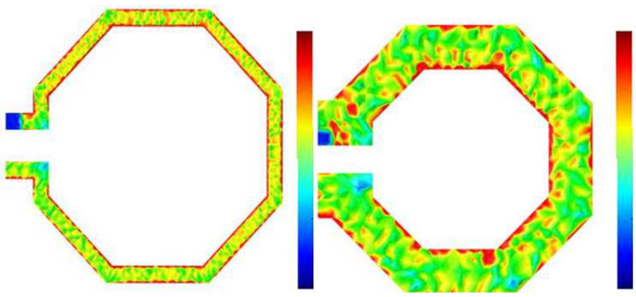

Figure 18. *Simulated current density at 100 MHz with different widths.*

In Figure 19, we observe 3D mesh of octagonal integrated transformer alone and with the different layers.

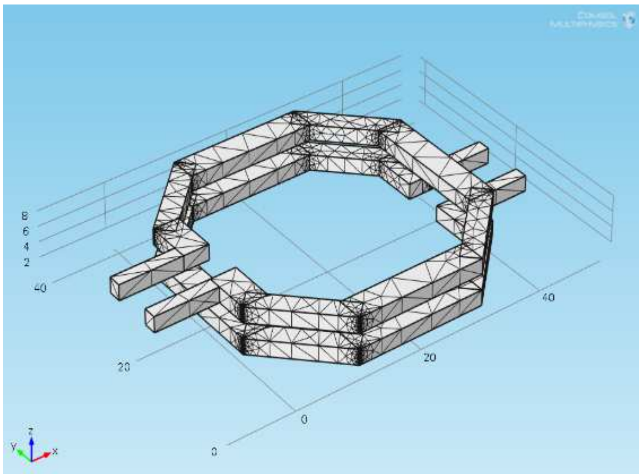

(a)

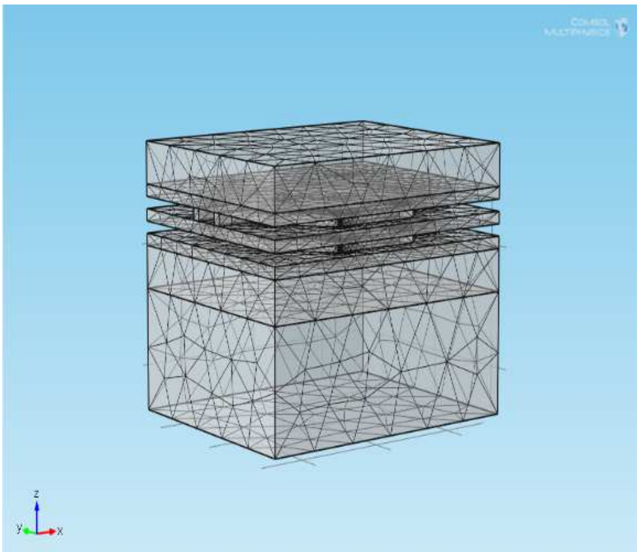

(b)

Figure 19. *3D mesh transformer: (a) Octagonal windings geometry, (b) Global structure.*

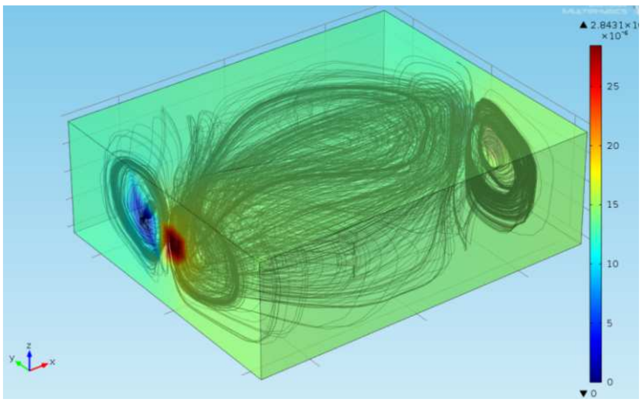

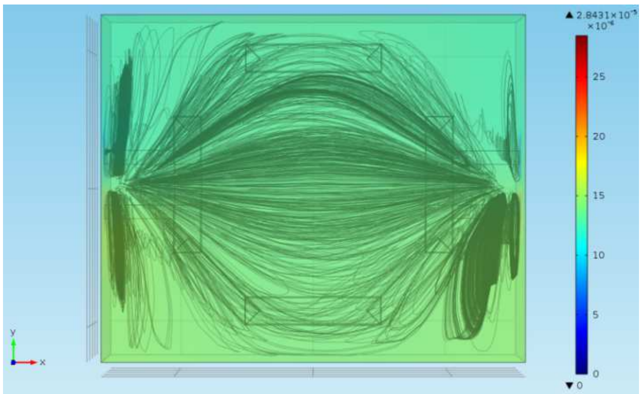

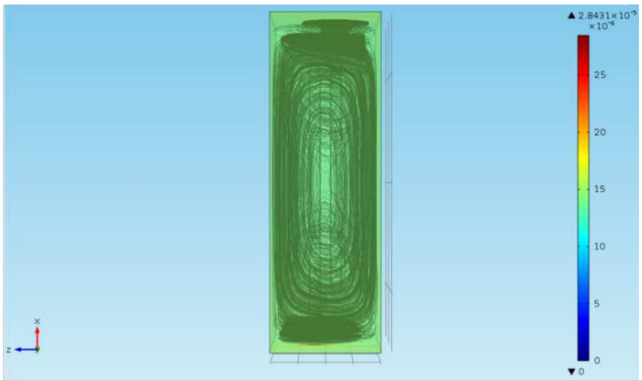

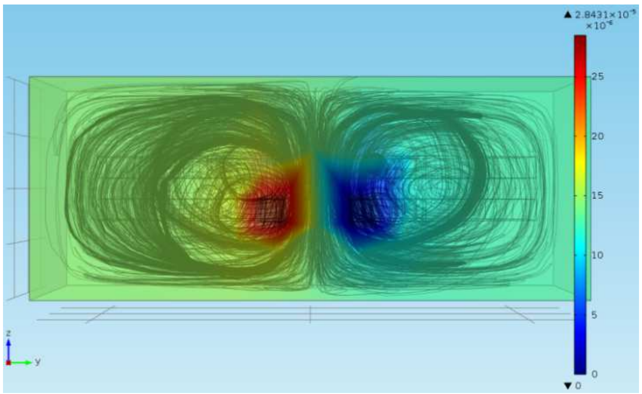

Figure 20. *Distribution of magnetic field in the transformer.*

Figure 20 shows the distribution of magnetic field in transformer composed of two octagonal windings of copper, deposited on ferrite NiZn magnetic layer and isolated by a dioxide layer, all these layers are deposited on a silicon substrate.

10. Conclusion

This paper present the design of RF transformer. The first considered parameter was the direction in which coupling between windings takes place. It was shown that a vertical coupling is more advantageous, as it provides distinctively better coupling coefficients and minimum insertion loss. Concerning the shape of windings, octagonal transformers were shown to present higher quality factors than their square counterparts. Moreover, the effect of the position of the feed lines of the two windings was investigated. It was shown that while flipped transformers can achieve lower losses, the non-flipped topology allows a stronger magnetic coupling and a more wideband behavior. The conclusion drawn in this paper constitute an important base to allow the definition of the best-suited topologies for application in specific integrated circuits. Moreover, the results obtained throughout this paper were taken into account in order to guide the development of an electric model for RF transformers.

References

[1] J. Aguilera, R. Berenguer, « Design and test of integrated inductors for RF applications », Kluwer Academic Publishers, 2004.

[2] B. Estibals, J. L. Sanchez, C. Alonso, H. Camon et J. P. Laur, «Vers l'intégration de convertisseurs pour l'alimentation des microsystèmes», J3EA, Journal sur l'Enseignement des sciences et technologies de l'information et des systèmes, Vol 2, 2003.

[3] Y. Maycvskiy, « Analysis and modeling of monolithic on-chip transformers on silicon substrates », Master Thesis, Oregon State University, United States of America, 10 June 2005.

[4] A. S. Ezzulddin, M. H. Ali, M. S. Abdulwahab, «On-chip RF transformer performance improvement technique», Eng. & Tech. Journal, Vol. 28, N°. 4, 2010.

[5] Z. Ouyang, Ole C. Thomsen, M. A. E. Andersen, «Optimal design and tradeoff analysis of planar transformer in high-power DC–DC converters», IEEE Transactions on Industrial Electronics, January 25, 2010.

[6] Xun Liu, S. Y. Ron Hui, "Equivalent Circuit Modeling of a Multilayer Planar Winding Array Structure for Use in a Universal Contactless Battery Charging Platform", IEEE transactions on power electronics, Vol. 22, No. 1, January 2007.

[7] N. M. Nguyen, R. G. Meyer, « Si IC-compatible inductors and LC passive filters», IEEE Journal of Solid-State Circuits (25) (1990) 1028–1031.

[8] K. B. Ashby, W. C. Finley, J. J. Bastek, S. Moinian, I. A. Koullias, «High Q inductors for wireless applications in a complementary silicon bipolar process», in: Proc. Bipolar/BiCMOS Circuits and Technology Meeting, 1994, pp. 179–182.

[9] C. Patrick Yue, S. Simon Wong, « Physical modeling of spiral inductors on silicon», IEEE Transactions on Electron Devices 47 (3) (2000).

[10] M. Yamaguchi, T. Kuribara, K.-I. Arai, «Two port type ferromagnetic RF integrated inductor», in: IEEE International Microwave Symposium, IMS-2002, TU3C-2, Seattle, USA, 2002, pp. 197–200.

[11] Ali Telli, Simsek Demir, Murat Askar, «Practical Performance of Planar Spiral Inductors». IEEE, 2004, pp. 487-490.

[12] Y. Benhadda, A. Hamid, T. Lebey, M. Derkaoui, «Design and modeling of an integrated inductor in a Buck converter DC-DC», Journal of Nano- and Electronic Physics, Vol. 7, No. 2, 10 June 2015.

[13] M. Derkaoui, R. Melati, A. Hamid, «Modeling of a planar inductor for converters low power», Global Conference on renewables and Energy Efficiency for Desert Regions GCREEDER'11, 2011, Jordanie.

[14] R. Melati, A. Hamid, T. Lebey, M. Derkaoui, «Design of a new electrical model of a ferromagnetic planar inductor for its integration in a micro-converter», Mathematical and Computer Modelling, Vol 57, pp 200–227, Janvier 2013.

[15] M. Derkaoui, A. Hamid, T. Lebey, R. Melati, «Design and modeling of an integrated transformer in a flyback converter», Telecommunication, Computing, Electronics and Control, TELKOMNIKA, SCOPUS Vol. 11, N° 4, pp. 669~682, December 2013. ISSN: 1693-6930.

[16] H-A. Wheeler & al., «Simple inductance formulas for radio coils», Proc. IRE, 16, n° 10, pp. 1398-1400.

[17] S. Mohan & al., «Simple Accurate Expressions for Planar Spiral Inductances», IEEE Journal of Solid -State Circuits, 34, n° 10 (1999), pp. 1419-1424.

[18] B. Estibals, A. Salles, «Design and realization of integrated inductor with low DC-resistance value for integrated power applications», HAIT Journal of Science and Engineering B, Vol. 2, Issues 5-6, pp. 848-868, 2005.

[19] ShwetabhVerma, Jose M. Cruz, « On-chip Inductors and Transformers », SMLI TR-99-79 December 1999.

[20] Y. K. Koutsoyannopoulos, «Systematic Analysis and Modeling of Integrated Inductors and Transformers in RF IC Design», Analog and Digital Signal Processing, Vol. 47, No. 8, August 2000 699.

[21] D. Belot, B. Leite, E. Kerherve, and J. B. Begueret, «Millimeter-wave transformer with a high transformation factor and a low insertion loss», U.S. Patent Application12/787,782, 2010.

[22] C. Wang, H. Liao, Y. Xiong, C. Li, R. Huang, and Y. Wang, «A physics-based equivalent-circuit model for on-chip symmetric transformers with accurate substrate modeling», IEEE Transactions on Microwave Theory and Techniques, vol. 57, no. 4, pp. 980–990, 2009.

[23] J. Gautier, «Modèles électriques pour la conception des circuits intégrés sur silicium», Lavoisier, 2004.